THE JOURNAL OF PHYSICAL CHEMISTRY A

Article

pubs.acs.org/JPCA

# Computational Study of Cyclohexanone–Monomer Co-initiation Mechanism in Thermal Homo-polymerization of Methyl Acrylate and Methyl Methacrylate

Shi Liu,[†] Sriraj Srinivasan,[‡] Michael C. Grady,[§] Masoud Soroush,[∥] and Andrew M. Rappe*,[†]

[†]The Makineni Theoretical Laboratories, Department of Chemistry, University of Pennsylvania, Philadelphia, Pennsylvania 19104-6323, United States

[‡]Arkema Inc., 900 First Avenue, King of Prussia, Pennsylvania 19406, United States

[§]DuPont Experimental Station, Wilmington, Delaware 19880-0308, United States

[∥]Department of Chemical and Biological Engineering, Drexel University, Philadelphia, Pennsylvania 19104, United States

Supporting Information

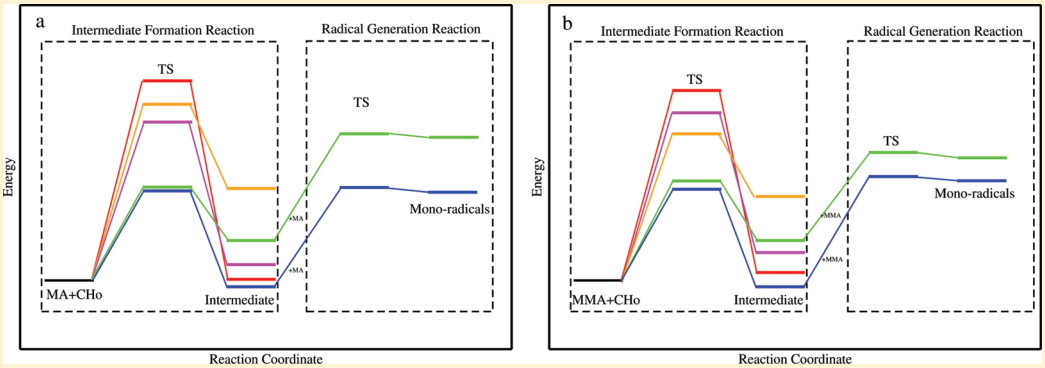


**ABSTRACT:** This paper presents a systematic computational study of the mechanism of cyclohexanone–monomer co-initiation in high-temperature homopolymerization of methyl acrylate (MA) and methyl methacrylate (MMA). Previous experimental studies of spontaneous thermal homopolymerization of MA and MMA showed higher monomer conversion in the presence of cyclohexanone than xylene. However, these studies did not reveal the initiation mechanism(s) or the initiating species. To identify the initiation mechanism and the initiating species, we explore four different mechanisms, (1) Kaim, (2) Flory, (3) $\alpha$-position hydrogen transfer, and (4) Mayo, using first-principles density functional theory (DFT) and second-order Møller–Plesset perturbation theory (MP2) calculations. Transition-state geometries for each mechanism are determined using B3LYP/6-31G* and assessed with MP2/6-31G*. Activation energies and rate constants are calculated using transition-state theory. The harmonic oscillator approximation and tunneling corrections are applied to compute the reaction rate constants. This study indicates that $\alpha$-position hydrogen transfer and Mayo mechanisms have comparable barriers and are capable of generating monoradicals for initiating polymerization of MA and MMA; these two mechanisms can cause cyclohexanone–monomer co-initiation in thermal polymerization of MA and MMA.

## 1. INTRODUCTION

Acrylate and methacrylate polymers are used in the production of paints, protective coatings and adhesives, due to their good adhesion, non-wettability, and photostability.[1,2] Stringent environmental regulations have mandated a reduction in the volatile organic content (VOC) of paints to less than 300 ppm.[2,3] To achieve this, the conventional high-solvent low-temperature (<100 °C) polymerization processes were replaced with low-solvent high-temperature (>100 °C) polymerization processes. High polymerization temperature speeds up secondary reactions such as spontaneous initiation, back-biting, and $\beta$-scission reactions. Spontaneous (no external initiator added) thermal polymerization of acrylates and methacrylates has been reported to be a promising approach to produce low-molecular-weight resins.[4] The absence of an external initiator reduces costs and improves end-product quality.[5,6]

Grady et al.[7] demonstrated that spontaneous high-temperature polymerization of acrylates could occur in the absence of any known initiators at temperatures above 373 K. Further studies[8] using electrospray ionization/Fourier transform mass spectrometry (ESI/FTMS) analysis indicated the autoinitiation behavior but were unable to identify the initiating species in the polymerization of alkyl acrylates. Junkers et al.[9] reported that highly uniform macromonomers with unsaturated end groups

Received: December 23, 2011
Revised: May 1, 2012
Published: May 1, 2012

  

are formed without addition of any external chain transfer agents in high-temperature autoinitiated polymerization of *n*-butyl acrylate (*n*BA). It is highly probable that the unsaturated end groups are key to sustaining polymerization, and consequently leading to the formation of complex polymer architectures.

High-temperature spontaneous polymerization of methyl methacrylate (MMA) has been widely studied.[10−17] Significant differences in high-temperature polymerization of MA and MMA have been reported.[8,13,18,19] Higher rates of chain transfer, lower dimer/trimer/oligomer formation, higher monomer conversion, and lower average molecular weights have been shown in thermal polymerization of MA than in MMA.

Two mechanisms for monomer self-initiation, the Mayo[20] and Flory[21] mechanisms, have been explored. Mayo proposed that a Diels−Alder adduct (DAA) is formed by two monomers and that the DAA is capable of donating a hydrogen atom to a third monomer so as to generate monoradicals for initiation. Flory suggested a diradical mechanism, in which a diradical intermediate formed during [2+2] thermal cycloaddition reaction has the ability to abstract a hydrogen from or lose a hydrogen to a third monomer to produce radical pairs, initiating the polymerization. Based on various types of experiments[11,13,14] and macroscopic mechanistic modeling,[18] it was proposed that Flory's diradical mechanism is the most probable monomer self-initiation mechanism in spontaneous thermal polymerization of MMA. Pryor and Laswell[22] postulated that the diradical species should be in its triplet state to form a monoradical. However, no conclusive evidence of the existence of the diradical species was provided. Recent studies using quantum chemical calculations (B3LYP and MP2) revealed that the Flory mechanism is most likely causing monomer self-initiation in methyl, ethyl and *n*-butyl acrylate[23,24] and methyl methacrylate.[25,26] The triplet diradical, formed via intersystem crossing from the singlet diradical, was found to be the key intermediate involved in the generation of monoradicals needed for initiation in high-temperature polymerization of alkyl acrylates and a key intermediate in polymerization of MMA. Results[19] from the matrix-assisted laser desorption/ionization time-of-flight (MALDI) analysis of poly(methyl acrylate) synthesized via spontaneous thermal polymerization at 140 °C is consistent with the proposed diradical mechanism.

Previous studies have shown that solvent can influence the initiation[19,27−29] step in thermal polymerization of acrylates and methacrylates. Ouchi et al.[30] found that several aldehydes could initiate the polymerization of methyl acrylate. Kaim[27,28] later reported that cyclohexanone (CHo) can also initiate polymerization of several vinyl monomers, such as acrylamide, *n*-butyl acrylate, and MMA. The Kaim initiation mechanism[28] involved the formation of a CHo−monomer complex, which then dissociates to release monoradicals for initiation. Xu et al. conducted atom transfer radical polymerization (ATRP) of MMA with $CuCl_2$/*N*,*N*,*N*′,*N*′,*N*″-pentamethyldiethylenetriamine (PMDTA) in various solvents and found that only in CHo, the polymerization achieved high conversion without the addition of any initiators.[29] A recent study[19] of spontaneous thermal polymerization of MA and *n*BA showed higher monomer conversion in CHo than in xylene and dimethyl sulfoxide. Before this study, there was no definitive evidence establishing the mechanism or the initiating species.

It has been reported that B3LYP/6-31G* can be a cost-effective and accurate method for the prediction of rate constants in free radical polymerization of alkyl acrylates and MMA.[24−26] Rate constants have been calculated using the transition-state theory (TST).[31] The harmonic oscillator (HO) approximation, in which all the vibrational modes are treated as harmonic springs, has been widely used to calculate the thermal and entropic correction factors that are required to predict the rate constants for various reactions. However, the HO approximation has been reported[32−37] to be inadequate to treat the low-frequency torsional modes, which correspond to anharmonic motions in the molecule. The rate constants calculated by applying the one-dimensional hindered rotor (1D-HR) model showed higher accuracy for the radical addition reaction of ethylbenzene radical to ethylene[34] and for the propagation reaction of ethylene,[35] methyl methacrylate, methyl acrylate,[37] and vinyl chloride.[33] But, identifying the rotational potentials can be computationally intensive for large molecules, and the lack of knowledge of the coupling between the rotors and vibrational modes can cause higher deviation of the estimated rate constants than that obtained using the HO approximation.[32] Previous studies on thermal polymerization of MMA and alkyl acrylates have shown that the use of MP2/6-31G* (to calculate the equilibrium geometries, frequencies and transition states) and the HO approximation can lead to the calculation of self-initiation rate constants that are comparable with experiments.[23,26] On the basis of these, we chose to use the HO approximation in this work. Ab initio calculations using a polarizable continuum model of chain propagation in free radical polymerization of acrylic acid and acrylates showed that the activation energies and transition-state structures are little different from those obtained via gas phase calculations.[38−40]

To the best of our knowledge, no computational study has been carried out to determine the mechanism of CHo−monomer co-initiation. This work uses quantum chemical calculations to systematically explore the Mayo,[20] Flory,[21] Kaim,[28] and $\alpha$-position hydrogen transfer mechanisms of initiation in thermal homopolymerization of MA and MMA in cyclohexanone. Transition-state geometries, activation barriers and rate constants are calculated for the reaction steps of the initiation mechanisms.

The rest of the paper is organized as follows. Section 2 discusses the computational methods used. Results and discussions are presented in section 3. Finally, concluding remarks are made in section 4.

## 2. COMPUTATIONAL METHOD

Calculations using the B3LYP/6-31G* level of theory were performed to identify the equilibrium geometries and transition-state structures. Reaction pathways were determined via intrinsic reaction coordinate (IRC) calculations in the forward and reverse directions. The IRC step size used in the calculations was 0.05 $(amu)^{1/2}$ Bohr. All the transition states and energy barriers were assessed using MP2/6-31G*. Calculations with larger basis sets were also carried out for selected reactions. Both the singlet- and triplet-state geometries were predicted using ROHF wave functions. The rate constant at a given temperature $T$, $k(T)$, was calculated using transition-state theory with

$$k(T) = \kappa(c^\circ)^{1-m}\frac{k_B T}{h}\exp\left(\frac{\Delta S^{\ddagger}}{R}\right)\exp\left(-\frac{\Delta H^{\ddagger}}{RT}\right) \quad (1)$$


dx.doi.org/10.1021/jp2124394 | J. Phys. Chem. A 2012, 116, 5337−5348

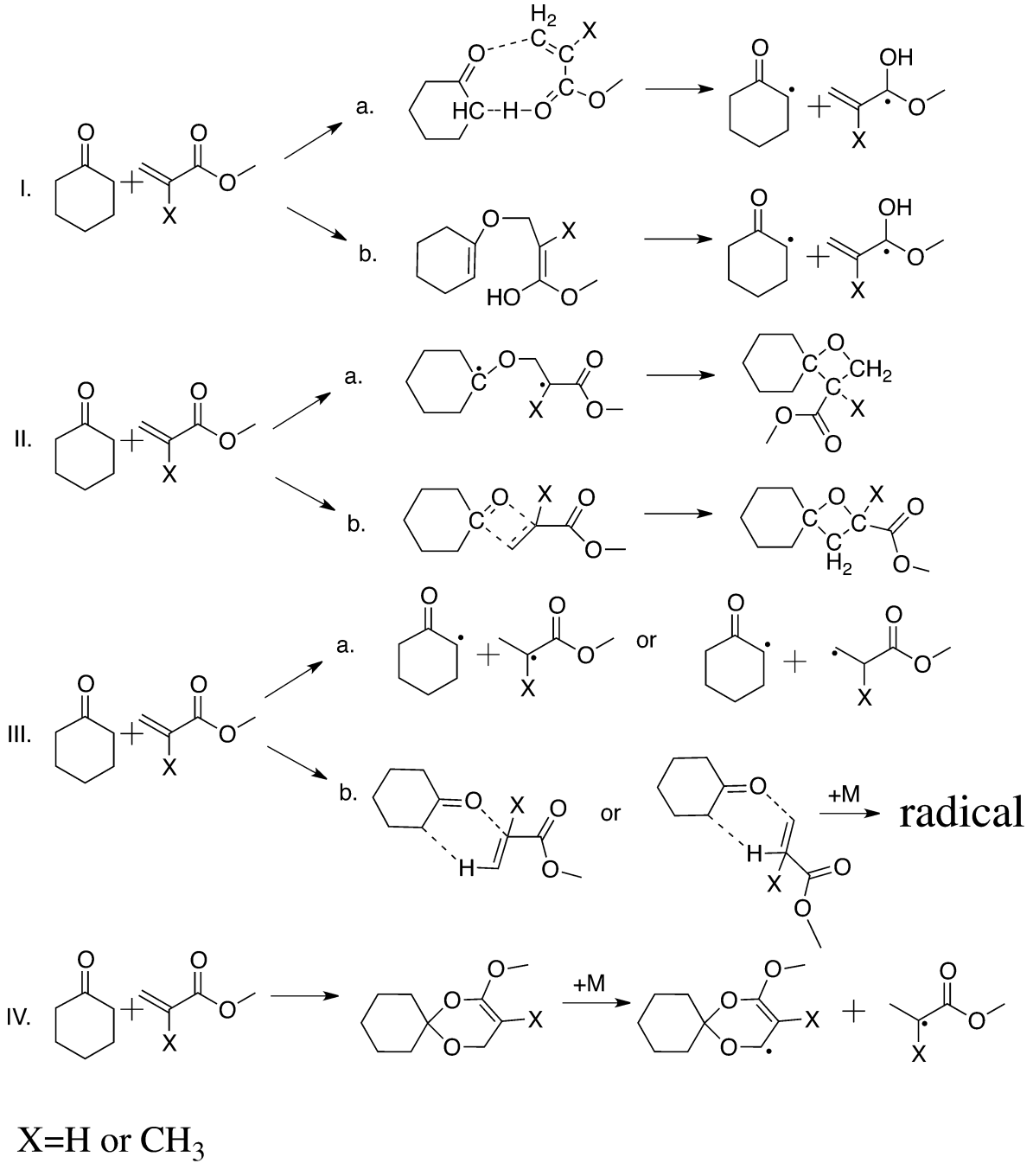


**Figure 1.** Cyclohexanone−monomer co-initiation mechanisms. I: (a) Mechanism proposed by Kaim, (b) Modified mechanism based on first-principles calculations. II: Flory mechanism (a) 2,2,3-cycloaddition (2,2,3,3-cycloaddition), (b) 2,2,4-cycloaddition (2,2,4,4-cycloaddition). III: $\alpha$-position hydrogen transfer reaction. IV: Mayo mechanism.

where $\kappa$ is the transmission coefficient, $c^\circ$ is the inverse of the reference volume assumed when the translational partition function is calculated, $m$ is the molecularity of the reaction, $k_B$ is the Boltzmann constant, $h$ is Planck's constant, $R$ is the universal gas constant, $\Delta S^\ddagger$ is the entropy of activation, and $\Delta H^\ddagger$ is the enthalpy of activation. $\Delta H^\ddagger$ is the sum of the energy difference between reactants and transition state ($E_0$), the zero-point vibrational energy (ZPVE) and the temperature correction ($\Delta\Delta H^\ddagger$):

$$\Delta H^\ddagger = E_0 + \mathrm{ZPVE} + \Delta\Delta H^\ddagger \tag{2}$$

Comparing eq 1 with the empirical Arrhenius expression for reaction rate coefficients,

$$k(T) = A \exp\left(\frac{-E_a}{RT}\right) \tag{3}$$

one can get the expressions for the frequency factor ($A$) and activation energy ($E_a$):

$$E_a = \Delta H^\ddagger + mRT \tag{4}$$

$$A = \kappa (c^\circ)^{1-m} \frac{k_B T}{h} e^m \exp\left(\frac{\Delta S^\ddagger}{R}\right) \tag{5}$$


dx.doi.org/10.1021/jp2124394 | J. Phys. Chem. A 2012, 116, 5337−5348

Based on previous studies,[23−26,41] the rigid rotor harmonic oscillator approximation[42] was used to construct partition functions, which are required for calculating ZPVE, $\Delta\Delta H^{\ddagger}$, and $\Delta S^{\ddagger}$. Appropriate scaling factors[43] (0.96 for B3LYP/6-31G* and 0.94 for MP2/6-31G*) were used. The Wigner[44] tunneling correction was calculated using

$$\kappa \approx 1 + \frac{1}{24}\left(\frac{h\nu^{\ddagger}}{k_B T}\right)^2 \quad (6)$$

where $\nu^{\ddagger}$ is the imaginary frequency of the transition state. Because the Eckart tunneling method has been reported[32,45−47] to be more accurate than the Wigner method, we also computed the rate coefficients with Eckart tunneling correction. The Eckart method is described in detail in the Supporting Information. All of our calculations were carried out using GAMESS.[48]

## 3. RESULTS AND DISCUSSION

We studied and screened many CHo−monomer co-initiation reaction mechanisms in terms of their activation energies. Mechanisms involving an endothermic reaction step with a heat of reaction higher than 300 kJ/mol were considered unlikely to contribute to CHo−monomer co-initiation in thermal polymerization of MA and MMA. The four mechanisms shown in Figure 1 passed this screening and were therefore selected for our detailed studies. The atom labels used throughout this paper are given in Chart 1.

**Chart 1. Atom Labels Used in This Computational Study**

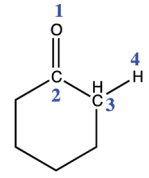


Cyclohexanone

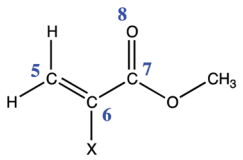


Methyl Methacrylate (X=$CH_3$) and Methyl Acrylate (X=H)

**3.1. Kaim Mechanism.** According to the mechanism proposed by Kaim,[27,28] which is shown in scheme Ia in Figure 1, the CHo−monomer complex formation occurs via simultaneous interactions between two types of atom pairs: the carbonyl oxygen (O8) of the monomer interacts with the $\alpha$-position hydrogen (H4) of CHo and the carbonyl group (O1) of CHo interacts with the vinyl carbon (C5) on the monomer. The decomposition of the weakly associated complex was postulated by Kaim to generate monoradicals for initiating polymerization.

To examine this proposed mechanism, three internuclear distances were constrained in the transition-state geometry search: 1.50 Å < $r$(O1—C5) < 2.50 Å, 1.10 Å < $r$(C3—H4) < 2.00 Å, and 1.10 Å < $r$(H4—O8) < 2.00 Å. We found that the monomer can form strong covalent bonds with the CHo, producing intermediate **3** for MA and intermediate **4** for MMA (Figure 2), rather than forming the weakly associated complex proposed by Kaim. The transition state, **1**, for the formation of the MA−CHo intermediate has $r$(O1—C5) = 1.79 Å, $r$(C3—H4) = 1.58 Å, and $r$(H4—O8) = 1.14 Å. As for the formation of the MMA−CHo intermediate, the transition-state structure **2** has $r$(O1—C5) = 1.61 Å, $r$(C3—H4) = 1.39 Å, and $r$(H4—O8) = 1.24 Å. IRC calculations starting at the transition states suggested that the formation of a covalent bond between O1 and C5 is favored. Validation with higher levels of theory, B3LYP/6-31G**, B3LYP/6-31+G*, B3LYP/6-31++G**,

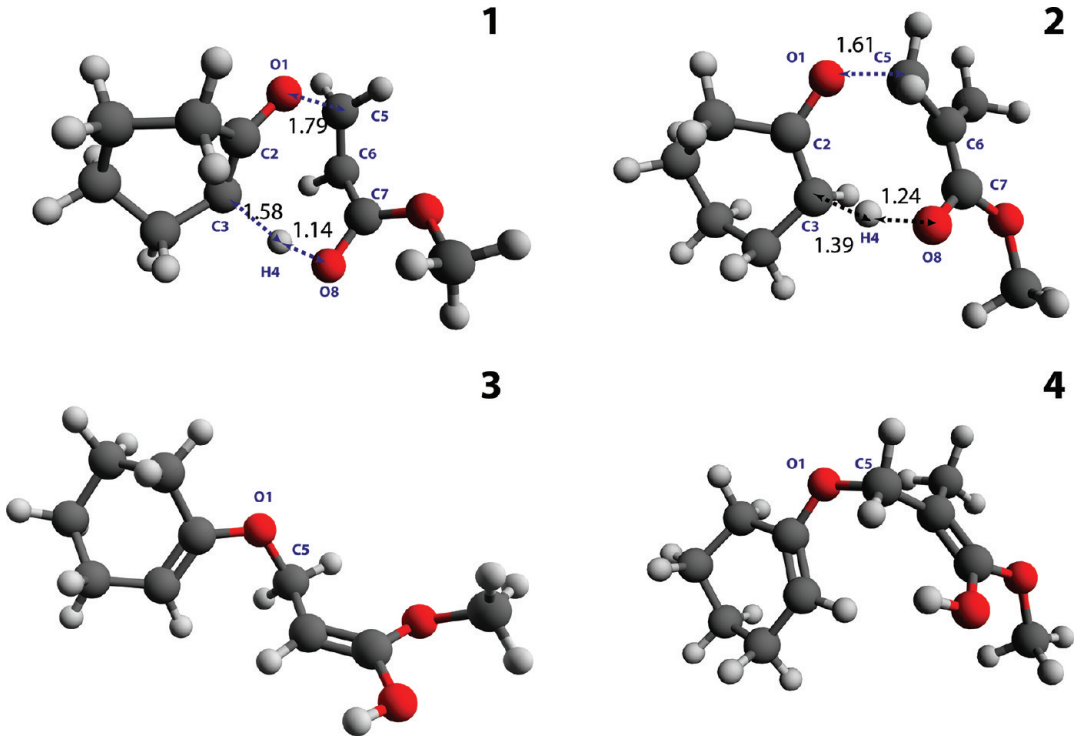


**Figure 2.** Transition states and monomer−CHo intermediate in the modified Kaim mechanism: **1**, transition state of MA−CHo intermediate formation; **2**, transition state of MMA−CHo intermediate formation; **3**, MA−CHo intermediate; **4**, MMA−CHo intermediate. All interatomic lengths are in Å.


dx.doi.org/10.1021/jp2124394 | J. Phys. Chem. A 2012, 116, 5337−5348

Table 1. Activation Energy ($E_a$), Activation Enthalpy ($\Delta H^{\ddagger}_{298K}$), and Activation Free Energy ($\Delta G^{\ddagger}_{298K}$) in kJ/mol; Tunneling Factors ($\kappa_W$ for Wigner Correction and $\kappa_E$ for Eckart Correction); and Frequency Factor ($A$) and Corresponding Rate Constants ($k_W$ and $k_E$) in $M^{-1}$ $s^{-1}$ at 298 K for the Modified Kaim Mechanism Using Different Levels of Theory

| species | level of Theory | $E_a$ | $\Delta H^{\ddagger}_{298K}$ | $\Delta G^{\ddagger}_{298K}$ | ln $A$ | $\kappa_W$ | $k_W$ | $\kappa_E$ | $k_E$ |
|---|---|---|---|---|---|---|---|---|---|
| MA + CHo | B3LYP/6-31G* | 254.11 | 249.15 | 304.05 | 12.51 | 2.26 | $1.84 \times 10^{-39}$ | 5.67 | $4.61 \times 10^{-39}$ |
| | B3LYP/6-31G** | 244.44 | 239.48 | 295.60 | 12.02 | 2.21 | $5.45 \times 10^{-38}$ | 5.15 | $1.27 \times 10^{-37}$ |
| | B3LYP/6-31+G* | 266.53 | 261.57 | 316.58 | 12.46 | 1.51 | $7.84 \times 10^{-42}$ | 1.76 | $9.14 \times 10^{-42}$ |
| | B3LYP/6-311G** | 254.25 | 249.29 | 304.92 | 12.21 | 2.31 | $1.33 \times 10^{-39}$ | 6.36 | $3.66 \times 10^{-39}$ |
| | B3LYP/6-311+G* | 272.97 | 268.01 | 322.91 | 12.51 | 2.52 | $1.02 \times 10^{-42}$ | 10.22 | $4.12 \times 10^{-42}$ |
| | B3LYP/6-311++G** | 261.77 | 256.81 | 312.30 | 12.27 | 2.32 | $6.78 \times 10^{-41}$ | 6.52 | $1.91 \times 10^{-40}$ |
| | MP2/6-31G* | 268.07 | 263.11 | 322.45 | 10.72 | 3.77 | $1.84 \times 10^{-42}$ | 608.46 | $2.97 \times 10^{-40}$ |
| | MP2/6-31G** | 258.64 | 253.68 | 314.09 | 10.29 | 3.78 | $5.37 \times 10^{-41}$ | 820.72 | $1.17 \times 10^{-38}$ |
| | MP2/6-31+G* | 261.44 | 256.49 | 315.85 | 10.71 | 3.79 | $2.65 \times 10^{-41}$ | 656.86 | $4.59 \times 10^{-39}$ |
| MMA + CHo | B3LYP/6-31G* | 212.97 | 208.01 | 268.90 | 10.09 | 2.91 | $3.42 \times 10^{-33}$ | 21.71 | $2.55 \times 10^{-32}$ |
| | B3LYP/6-31G** | 204.82 | 199.86 | 261.04 | 9.98 | 2.84 | $7.96 \times 10^{-32}$ | 18.64 | $5.21 \times 10^{-31}$ |
| | B3LYP/6-31+G* | 225.28 | 220.32 | 281.96 | 9.79 | 2.98 | $1.80 \times 10^{-35}$ | 26.38 | $1.59 \times 10^{-34}$ |
| | B3LYP/6-31++G** | 217.47 | 212.51 | 273.82 | 9.92 | 2.88 | $4.66 \times 10^{-34}$ | 21.05 | $3.41 \times 10^{-33}$ |
| | B3LYP/6-311G** | 218.06 | 213.11 | 273.15 | 10.43 | 2.94 | $6.23 \times 10^{-34}$ | 25.76 | $5.47 \times 10^{-33}$ |
| | B3LYP/6-311+G* | 233.92 | 228.96 | 286.84 | 11.30 | 3.15 | $2.66 \times 10^{-36}$ | 41.80 | $3.53 \times 10^{-35}$ |
| | MP2/6-31G* | 224.90 | 219.94 | 279.46 | 10.65 | 3.33 | $5.52 \times 10^{-35}$ | 89.65 | $1.49 \times 10^{-33}$ |
| | MP2/6-31G** | 216.89 | 211.93 | 272.95 | 10.04 | 3.32 | $7.60 \times 10^{-34}$ | 94.21 | $2.16 \times 10^{-32}$ |
| | MP2/6-31+G* | 219.62 | 214.66 | 273.04 | 11.11 | 3.31 | $7.33 \times 10^{-34}$ | 57.76 | $1.28 \times 10^{-32}$ |

**Chart 2. Products of [2+2] Cycloaddition**

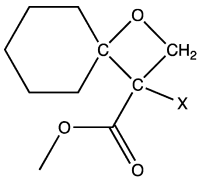


2,2,3-substituted oxetane (X=H)
2,2,3,3-substituted oxetane (X=$CH_3$)

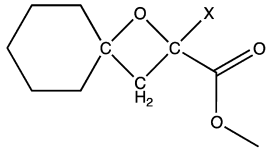


2,2,4-substituted oxetane (X=H)
2,2,4,4-substituted oxetane (X=$CH_3$)

B3LYP/6-311G**, B3LYP/6-311+G*, B3LYP/6-311++G**, MP2/6-31G**, and MP2/6-31+G*, all confirmed that the transition state leads to the O1—C5 bond formation. Mulliken population analysis was performed to understand the effect of O1—C5 interaction. Owing to the interaction between the O1 and C5, the charge on C6 of structure **1** becomes more negative, decreasing from −0.130 to −0.248, and the charge on C6 of structure **2** becomes less positive, reducing from 0.130 to 0.018. Due to the conjugation of C5═C6 and C7═O8, the

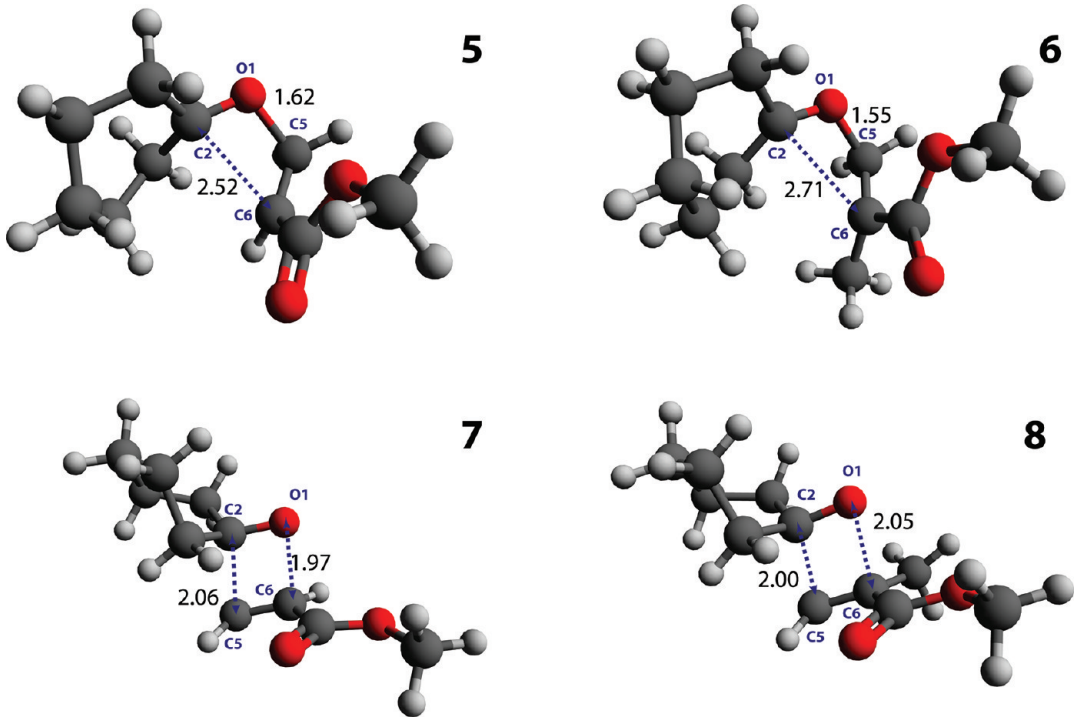


**Figure 3.** Transition states in the Flory mechanism: **5**, transition state of 2,2,3-cycloaddition of MA and CHo; **6**, transition state of 2,2,3,3-cycloaddition of MMA and CHo; **7**, transition state of 2,2,4-cycloaddition of MA and CHo; **8**, transition state of 2,2,4,4-cycloaddition of MMA and CHo. All interatomic lengths are in Å.


dx.doi.org/10.1021/jp2124394 | J. Phys. Chem. A 2012, 116, 5337−5348

**Table 2. Activation Energy ($E_a$), Activation Enthalpy ($\Delta H^{\ddagger}_{298K}$), and Activation Free Energy ($\Delta G^{\ddagger}_{298K}$) in kJ/mol; Tunneling Factors ($\kappa_W$ for Wigner Correction and $\kappa_E$ for Eckart Correction); and Frequency Factor ($A$) and Corresponding Rate Constants ($k_W$ and $k_E$) in $M^{-1}$ $s^{-1}$ at 298 K for the Flory Mechanism Using B3LYP/6-31G* and MP2/6-31G***

| species | reaction | level of theory | $E_a$ | $\Delta H^{\ddagger}_{298K}$ | $\Delta G^{\ddagger}_{298K}$ | ln $A$ | $\kappa_W$ | $k_W$ | $\kappa_E$ | $k_E$ |
|---|---|---|---|---|---|---|---|---|---|---|
| MA + CHo | 2,2,3-cycloaddition | B3LYP/6-31G* | 228.09 | 223.14 | 278.84 | 12.18 | 1.78 | $3.80 \times 10^{-35}$ | 2.58 | $5.51 \times 10^{-35}$ |
| | | MP2/6-31G* | 231.37 | 226.41 | 284.07 | 11.40 | 1.97 | $5.10 \times 10^{-36}$ | 3.49 | $9.04 \times 10^{-36}$ |
| | 2,2,4-cycloaddition | B3LYP/6-31G* | 287.66 | 282.70 | 338.06 | 12.32 | 2.49 | $2.24 \times 10^{-45}$ | 11.15 | $9.99 \times 10^{-45}$ |
| | | MP2/6-31G* | 269.41 | 264.45 | 324.14 | 10.58 | 2.00 | $4.93 \times 10^{-43}$ | 3.70 | $9.12 \times 10^{-43}$ |
| MMA + CHo | 2,2,3,3-cycloaddition | B3LYP/6-31G* | 240.96 | 236.00 | 291.74 | 12.17 | 1.30 | $1.52 \times 10^{-37}$ | 1.38 | $1.61 \times 10^{-37}$ |
| | | MP2/6-31G* | 241.39 | 236.43 | 297.33 | 10.09 | 1.42 | $1.74 \times 10^{-38}$ | 1.58 | $1.94 \times 10^{-38}$ |
| | 2,2,4,4-cycloaddition | B3LYP/6-31G* | 271.34 | 266.38 | 323.94 | 11.43 | 2.32 | $6.18 \times 10^{-43}$ | 7.02 | $1.87 \times 10^{-42}$ |
| | | MP2/6-31G* | 246.51 | 241.55 | 303.69 | 9.59 | 2.07 | $1.95 \times 10^{-39}$ | 4.20 | $3.96 \times 10^{-39}$ |

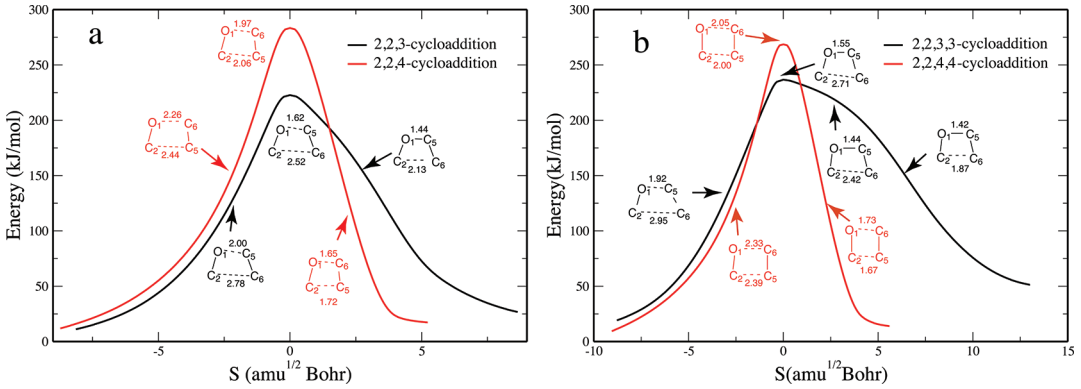


**Figure 4.** Intrinsic reaction coordinate path for the Flory mechanism. (a) 2,2,3- and 2,2,4-cycloaddition of MA and CHo; (b) 2,2,3,3- and 2,2,4,4-cycloaddition of MMA and CHo. All interatomic lengths are in Å.

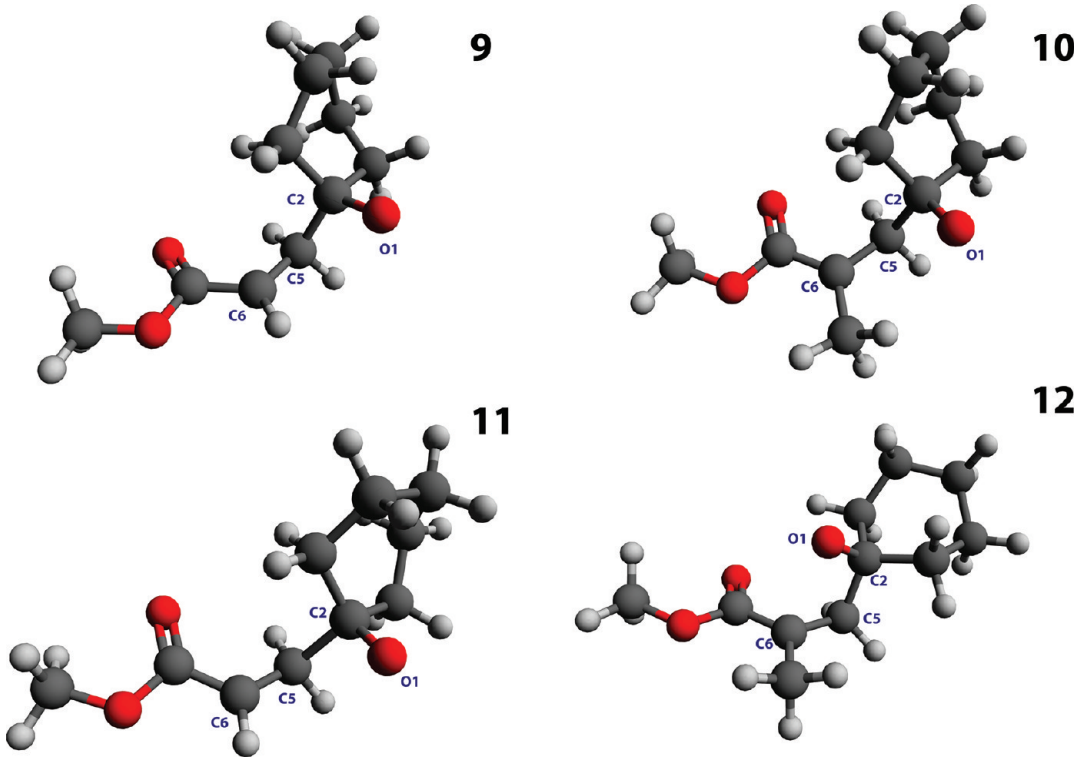


**Figure 5.** Triplet diradicals and minimum energy crossing point (MECP) in 2,2,4-cycloaddition of MA and 2,2,4,4-cycloaddition of MMA: **9**, triplet diradical of MA and CHo; **10**, Triplet diradical of MMA and CHo; **11**, MECP in 2,2,4-cycloaddition of MA and CHo; **12**, MECP in 2,2,4,4-cycloaddition of MMA and CHo.

electron density of O8 in turn changes from −0.489 to −0.593 in structure **1** and from −0.490 to −0.631 in structure **2**. Generally, a more negative charge (high electron density) means higher reactivity (toward proton abstraction), whereas a


dx.doi.org/10.1021/jp2124394 | J. Phys. Chem. A 2012, 116, 5337−5348

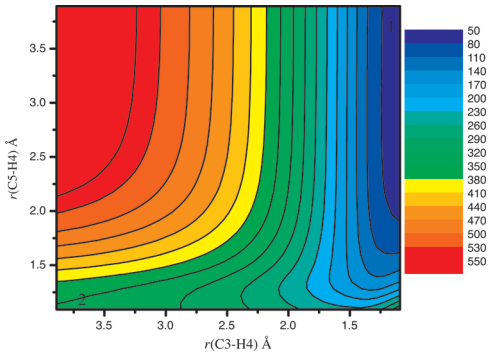


**Figure 6.** Contour map of the potential energy surface for direct hydrogen transfer from CHo to the $CH_2$-end of MA. All energies are relative to that of the reactant (CHo and MA) in kJ $mol^{-1}$. Structure 1 is weakly interacting CHo and MA. Structure 2 is a pair of monoradicals.

more positive charge (lower electron density) characterizes lower reactivity. Therefore, O8 becomes more electronegative because of the O1—C5 interaction and is more capable of abstracting the slightly acidic $\alpha$-position hydrogen of CHo. After cyclic covalent bond rearrangement, the MA−CHo intermediate **3** has $r$(O1—C5) = 1.44 Å and the MMA−CHo intermediate **4** has $r$(O1—C5) = 1.44 Å. Table 1 provides the energy barriers and rate constants for intermediate formation. The energy barriers predicted with larger basis sets show little difference (±15 kJ/mol) in the values compared to that of B3LYP/6-31G*. This indicates that B3LYP/6-31G* is a reliable level of theory with reasonable accuracy. We found that formation of the monomer−CHo intermediate has a high energy barrier, 254 kJ/mol for MA and 213 kJ/mol for MMA. Furthermore, the generation of radicals proposed by Kaim (starting from the intermediate we predict to form) would require the breaking of O1—C5 covalent bond in the intermediate, and the energy barrier is greater than 300 kJ/mol for thermal dissociation. This suggests that the formation of monoradicals via the dissociation of monomer−CHo intermediate is energetically unfavorable and, consequently, Kaim's mechanism is least likely to occur. The modified Kaim mechanism is shown in scheme Ib in Figure 1.

**3.2. Flory Mechanism.** Two types of cycloaddition reaction involving the carbonyl group C2═O1 of CHo and C5═C6 of MA and MMA are shown in Figure 1(II). Chart 2 shows the structures of the products in [2+2] cycloaddition. We name the reaction producing 2,2,3-substituted oxetane for MA (2,2,3,3-substituted oxetane for MMA) as 2,2,3-cycloaddition (2,2,3,3-cycloaddition), and the one producing 2,2,4-substituted oxetane for MA (2,2,4,4-substituted oxetane for MMA) as 2,2,4-cycloaddition (2,2,4,4-cycloaddition). The potential energy surface for these reactions was explored by constraining 1.45 Å < $r$(O1—C5) < 2.85 Å and 1.55 Å < $r$(C2—C6) < 2.85 Å for the 2,2,3-cycloaddition(2,2,3,3-cycloaddition), and 1.45 Å < $r$(O1—C6) < 2.85 Å and 1.55 Å < $r$(C2—C5) < 2.85 Å for the 2,2,4-cycloaddition (2,2,4,4-cycloaddition), respectively. The structures of the transition states are shown in Figure 3.

*Methyl Acrylate.* For the 2,2,3-cycloaddition, we located a nonconcerted transition state, **5**, with $r$(O1−C5) = 1.62 Å, $r$(C2−C6) = 2.52 Å, and Φ(C6−C5−O1−C2) = −29°. The estimated energy barriers using B3LYP and MP2/6-31G* are given in Table 2. They are significantly higher than that of the MA-MA [2+2] cycloaddition in monomer self-initiation.[23]

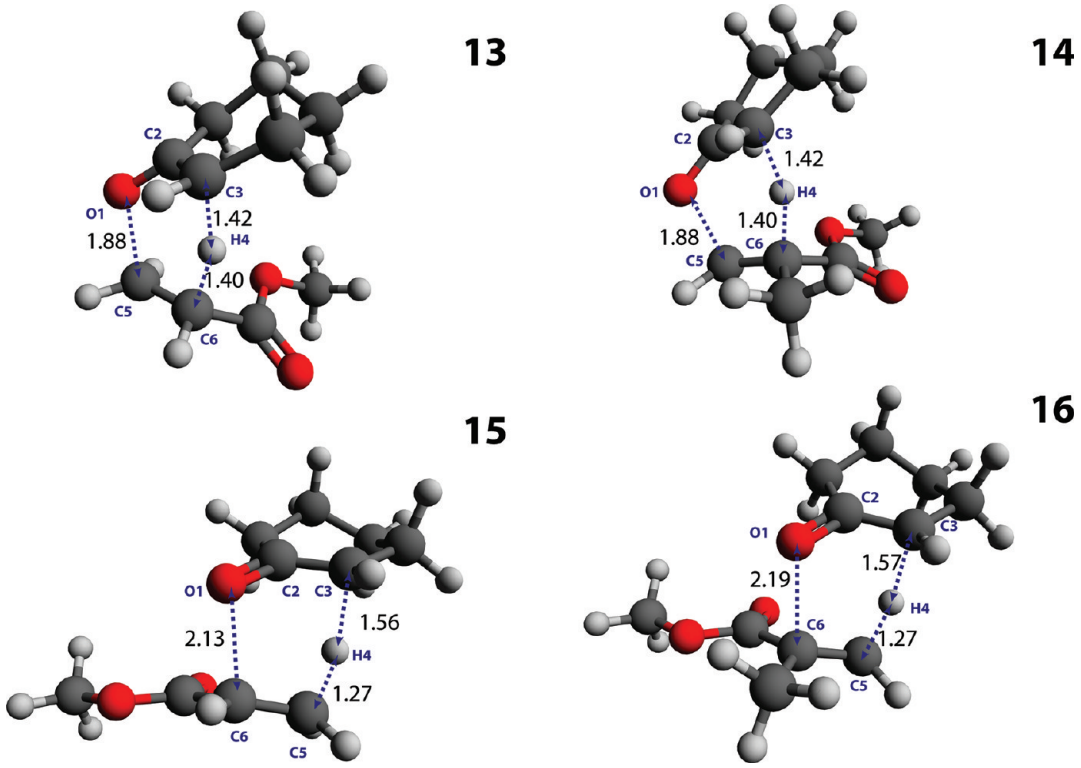


**Figure 7.** Transition states of the complexation-involved hydrogen transfer reactions: **13**, transition state of Anti-Markovnikov addition of MA and CHo; **14**, transition state of Anti-Markovnikov addition of MMA and CHo; **15**, transition state of Markovnikov addition of MA and CHo; **16**, transition state of Markovnikov addition of MMA and CHo. All interatomic lengths are in Å.


dx.doi.org/10.1021/jp2124394 | J. Phys. Chem. A 2012, 116, 5337−5348

Table 3. Activation Energy ($E_a$), Activation Enthalpy ($\Delta H^{\ddagger}_{298K}$), and Activation Free Energy ($\Delta G^{\ddagger}_{298K}$) in kJ/mol; Tunneling Factors ($\kappa_W$ for Wigner Correction and $\kappa_E$ for Eckart Correction); and Frequency Factor ($A$) and Corresponding Rate Constants ($k_W$ and $k_E$) in $M^{-1}$ $s^{-1}$ at 298 K for the Complexation-Involved $\alpha$-Position Hydrogen Transfer Reaction Using B3LYP/6-31G* and MP2/6-31G*

| species | mechanism | level of theory | $E_a$ | $\Delta H^{\ddagger}_{298K}$ | $\Delta G^{\ddagger}_{298K}$ | ln $A$ | $\kappa_W$ | $k_W$ | $\kappa_E$ | $k_E$ |
|---|---|---|---|---|---|---|---|---|---|---|
| MA + CHo | anti-Markovnikov | B3LYP/6-31G* | 144.57 | 139.61 | 197.43 | 11.33 | 2.59 | $1.01 \times 10^{-20}$ | 11.79 | $4.60 \times 10^{-20}$ |
| | | MP2/6-31G* | 128.91 | 123.96 | 182.99 | 10.84 | 2.29 | $3.03 \times 10^{-18}$ | 6.02 | $7.97 \times 10^{-18}$ |
| | Markovnikov | B3LYP/6-31G* | 133.44 | 128.49 | 185.45 | 11.68 | 1.73 | $8.51 \times 10^{-19}$ | 2.39 | $1.18 \times 10^{-18}$ |
| | | MP2/6-31G* | 118.88 | 113.93 | 169.88 | 12.08 | 1.37 | $3.59 \times 10^{-16}$ | 1.51 | $3.96 \times 10^{-16}$ |
| MMA + CHo | anti-Markovnikov | B3LYP/6-31G* | 155.04 | 150.08 | 205.61 | 12.25 | 2.54 | $3.67 \times 10^{-22}$ | 10.68 | $1.55 \times 10^{-21}$ |
| | | MP2/6-31G* | 129.04 | 124.08 | 183.23 | 10.79 | 2.13 | $2.56 \times 10^{-18}$ | 4.46 | $5.36 \times 10^{-18}$ |
| | Markovnikov | B3LYP/6-31G* | 129.90 | 124.94 | 185.51 | 10.22 | 1.61 | $7.68 \times 10^{-19}$ | 2.00 | $9.54 \times 10^{-19}$ |
| | | MP2/6-31G* | 103.90 | 98.94 | 159.03 | 10.42 | 1.34 | $2.81 \times 10^{-14}$ | 1.45 | $3.04 \times 10^{-14}$ |

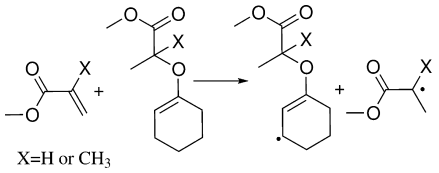


**Figure 8.** Monoradical generation reaction from the $CH_2$-end added intermediate.

Previous studies suggested that nonconcerted cycloaddition can arise from a stepwise biradical mechanism.[23,41] However, we found no energy-minimum singlet diradical intermediate. The occurrence of crossover from a higher energy singlet diradical to a lower energy triplet diradical was reported in monomer self-initiation of MA.[23] Here, we identified a triplet diradical with a structure similar to that of the nonconcerted transition state. We found that the energy of the triplet diradical is higher than that of the singlet transition state by 18.9 kJ/mol. This indicates that the intersystem crossing cannot be energetically favored. Based on these, we believe that the occurrence of intersystem crossing of the singlet diradical transition state to an active triplet diradical has lower probability than the production of inactive 2,2,3-substituted oxetane.

In the 2,2,4-cycloaddition reaction, we found no nonconcerted transition state. This can be attributed to the instability of the nonconcerted transition state which had radical center located upon the secondary carbon (C5) or the oxygen atom (O1). We identified the presence of a concerted transition state, **7**, with $r$(O1−C6) = 1.97 Å, $r$(C2−C5) = 2.06 Å and Φ(C5−C6−O1−C2) = 7.1°. The activation energy of the concerted 2,2,4-cycloaddition was calculated using B3LYP and found to be greater than that of nonconcerted 2,2,3-cycloaddition. This indicates that the concerted pathway is less preferred, which agrees with the rules of Woodward and Hoffmann for [2+2] cycloaddition. The rules state that the formation of concerted transition state is thermally forbidden. It can be seen from the minimum energy reaction path shown in Figure 4a that the concerted pathway has higher energy barrier, and the ring closure occurs earlier in the reaction coordinate, in comparison to the nonconcerted pathway. We located a stable triplet diradical intermediate, **9**, which resembles the geometry of the concerted singlet transition state (Figure 5). The energy of triplet diradical, **9**, is lower than that of the concerted transition state, **7**, by 51 kJ/mol. The minimum energy crossing point (MECP) between the singlet transition state and the triplet diradical was obtained using B3LYP/6-31G*. The geometry at the MECP, **11**, is $r$(C2−C5) = 1.71 Å, $r$(O1−C6) = 3.07 Å, and Φ(C6−C5−C2−O1) = 61.24°, and the energy of the MECP structure is 264 kJ/mol higher than that of the reactants.

*Methyl Methacrylate.* In the 2,2,3,3-cycloaddition reaction, we determined the presence of a nonconcerted transition state, **6**, with $r$(O1−C5) = 1.55 Å, $r$(C2−C6) = 2.71 Å, and Φ(C6−C5−O1−C2) = −42.7°, but no stable singlet diradical intermediate was found. This can be attributed to the lack of electron delocalization within the ring structure to stabilize the radical. The energy of the triplet diradical of MMA−CHo is higher than that of the singlet diradical transition state. Due to this, crossover of the diradical from singlet to triplet state is unlikely in the nonconcerted 2,2,3,3-cycloaddition. This agrees with the 2,2,3-cycloaddition mechanism in MA−CHo.

The transition-state structure **8** for 2,2,4,4-cycloaddition has $r$(O1−C6) = 2.05 Å, $r$(C2−C5) = 2.00 Å, and Φ(C5−C6−O1−C2) = 4.2°. Figure 4b presents IRC plots of 2,2,3,3- and 2,2,4,4-cycloaddition in MMA. Using B3LYP, the energy barrier of the 2,2,4,4-cycloaddition was estimated to be 30 kJ/mol higher than that of the 2,2,3,3-cycloaddition, which indicates that the 2,2,3,3-cycloaddition is energetically favored. A triplet diradical, **10**, with 44.6 kJ/mol less energy than the singlet transition state, **8**, was found. The energy of the MECP, **12**, with $r$(C2−C5) = 1.56 Å, $r$(O1−C6) = 2.32 Å, and Φ(C6−

Table 4. Activation Energy ($E_a$), Activation Enthalpy ($\Delta H^{\ddagger}_{298K}$), and Activation Free Energy ($\Delta G^{\ddagger}_{298K}$) in kJ/mol; Wigner Tunneling Factor ($\kappa_W$); and Frequency Factor ($A$) and Rate Constant ($k_W$) in $M^{-1}$ $s^{-1}$ at 298 K for the Mono-Radical Generation Reaction from the $CH_2$-End Added Intermediate and DAA Using B3LYP/6-31G* [a]

| intermediate | monomer | $E_a$ | $\Delta H^{\ddagger}_{298K}$ | $\Delta G^{\ddagger}_{298K}$ | ln $A$ | $\kappa_W$ | $k_W$ | $k_r$ |
|---|---|---|---|---|---|---|---|---|
| $CH_2$-end added | MA | 132.2 | 127.3 | 177.1 | 14.5 | 1.12 | $1.54 \times 10^{-17}$ | 5.25 |
| | MMA | 160.8 | 155.8 | 217.9 | 9.6 | 1.67 | $1.12 \times 10^{-24}$ | $1.56 \times 10^{-4}$ |
| DAA | MA | 118.9 | 113.9 | 170.5 | 11.8 | 1.16 | $3.29 \times 10^{-16}$ | 19.10 |
| | MMA | 128.0 | 123.1 | 180.7 | 11.4 | 1.36 | $4.49 \times 10^{-18}$ | 1.54 |

[a] $k_r$ is the relative overall reaction rate coefficient compared to monomer-self initiation.


dx.doi.org/10.1021/jp2124394 | J. Phys. Chem. A 2012, 116, 5337−5348

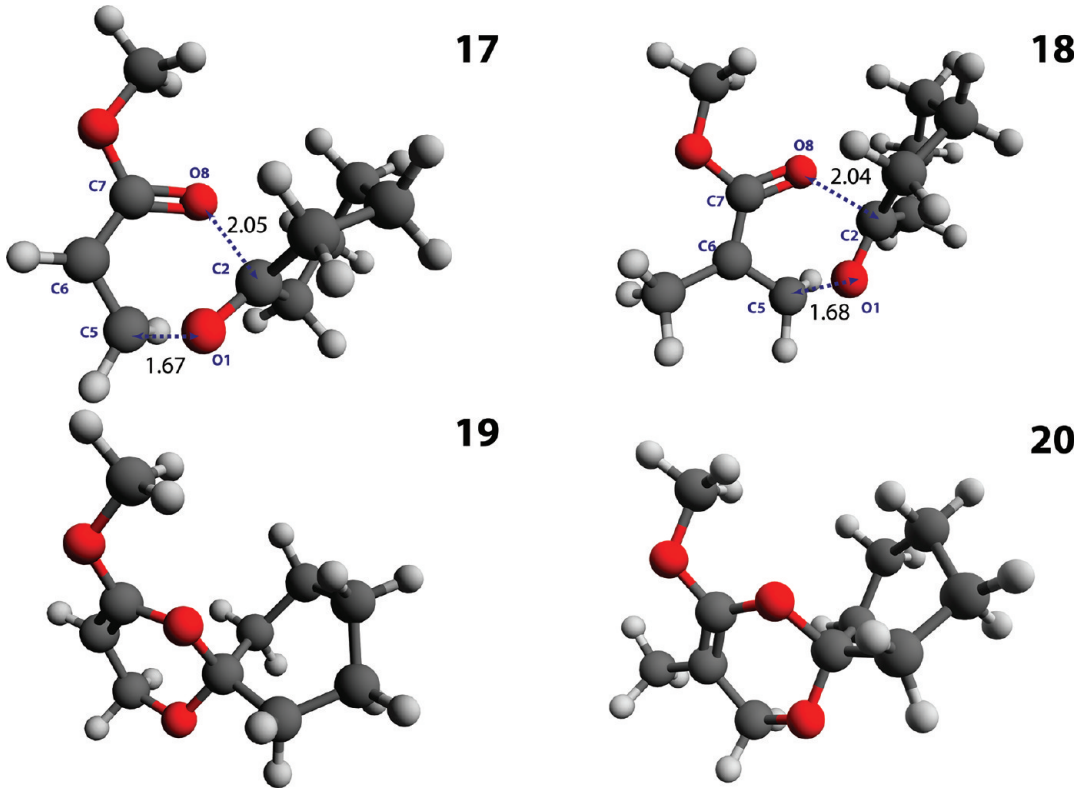


**Figure 9.** Transition states and Diels–Alder Adduct (DAA) in the Mayo mechanism: **17**, transition state of cycloaddition [4+2] of CHo and MA; **18**, transition state of cycloaddition [4+2] of CHo and MMA; **19**, DAA of CHo and MA; **20**, DAA of CHo and MMA. All interatomic lengths are in Å.

**Table 5. Activation Energy ($E_a$), Activation Enthalpy ($\Delta H^{\ddagger}_{298K}$), and Activation Free Energy ($\Delta G^{\ddagger}_{298K}$) in kJ/mol; Tunneling Factors ($\kappa_W$ for Wigner Correction and $\kappa_E$ for Eckart Correction); and Frequency Factor ($A$) and Corresponding Rate Constants ($k_W$ and $k_E$) in $M^{-1}$ $s^{-1}$ at 298 K for the Formation of a Diels–Alder Adduct Using B3LYP/6-31G* and MP2/6-31G***

| species | level of theory | $E_a$ | $\Delta H^{\ddagger}_{298K}$ | $\Delta G^{\ddagger}_{298K}$ | ln $A$ | $\kappa_W$ | $k_W$ | $\kappa_E$ | $k_E$ |
|---|---|---|---|---|---|---|---|---|---|
| MA + CHo | B3LYP/6-31G* | 133.16 | 128.21 | 188.84 | 10.19 | 1.16 | $1.45 \times 10^{-19}$ | 1.19 | $1.49 \times 10^{-19}$ |
| | MP2/6-31G* | 128.91 | 123.96 | 188.36 | 8.67 | 1.32 | $2.00 \times 10^{-19}$ | 1.41 | $2.14 \times 10^{-19}$ |
| MMA + CHo | B3LYP/6-31G* | 141.44 | 136.48 | 199.09 | 9.40 | 1.17 | $2.35 \times 10^{-21}$ | 1.20 | $2.41 \times 10^{-21}$ |
| | MP2/6-31G* | 132.11 | 127.15 | 190.31 | 9.18 | 1.33 | $9.20 \times 10^{-20}$ | 1.43 | $9.89 \times 10^{-20}$ |

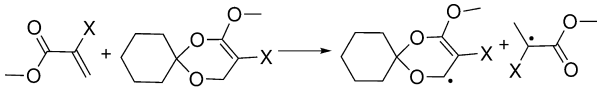


**Figure 10.** Hydrogen transfer reaction from DAA to a second monomer.

C5–C2–O1) = 3.89° is 241 kJ/mol higher than that of the reactants.

We predict that the occurrence of CHo-involved Flory mechanism to initiate polymerization of MA and MMA is less likely due to (a) the significantly higher energy barrier of the 2,2,4-cycloaddition (2,2,4,4-cycloaddition) than the 2,2,3-cycloaddition (2,2,3,3-cycloaddition) mechanism and (b) the additional energy barrier for the singlet diradical transition state in the 2,2,3-cycloaddition (2,2,3,3-cycloaddition) to cross over to the reactive triplet state and consequently generate monoradicals.

**3.3. α-Position Hydrogen Transfer.** This mechanism involves the transfer of an α-position hydrogen (e.g., H4) of CHo to the unsaturated C5═C6 of MA and MMA, as shown in Figure 1(III). Two types of α-position hydrogen transfer mechanisms, (a) direct hydrogen transfer reaction (scheme IIIa in Figure 1) and (b) complexation-involved hydrogen transfer reaction (scheme IIIb in Figure 1), were explored. The direct hydrogen transfer reaction, a reverse radical disproportionation, involves the transfer of an α-position hydrogen to a vinyl carbon atom (C5 or C6) of the monomer to form monoradicals. The complexation-involved hydrogen transfer reaction consists of the formation of a monomer–CHo intermediate via interactions between the carbonyl group (O1) of CHo and one unsaturated carbon atom C5 (or C6), and hydrogen transfer from CHo to another unsaturated carbon atom C6 (or C5). The hydrogen transfer to the $CH_2$ group (C5) is called Markovnikov addition, and that to CR(X)-end (C6) is known as anti-Markovnikov addition. Monoradical formation via hydrogen abstraction from the formed monomer–CHo intermediate to a second monomer was also studied.

We studied the direct transfer reaction by constraining 1.09 Å < $r$(C3–H4) < 3.89 Å and 1.09 Å < $r$(H4–C5) < 3.89 Å for Markovnikov addition and 1.09 Å < $r$(C3–H4) < 1.60 Å and 1.09 Å < $r$(H4–C6) < 1.60 Å for anti-Markovnikov addition. Figure 6 presents the 2D potential energy surface for


dx.doi.org/10.1021/jp2124394 | J. Phys. Chem. A 2012, 116, 5337–5348

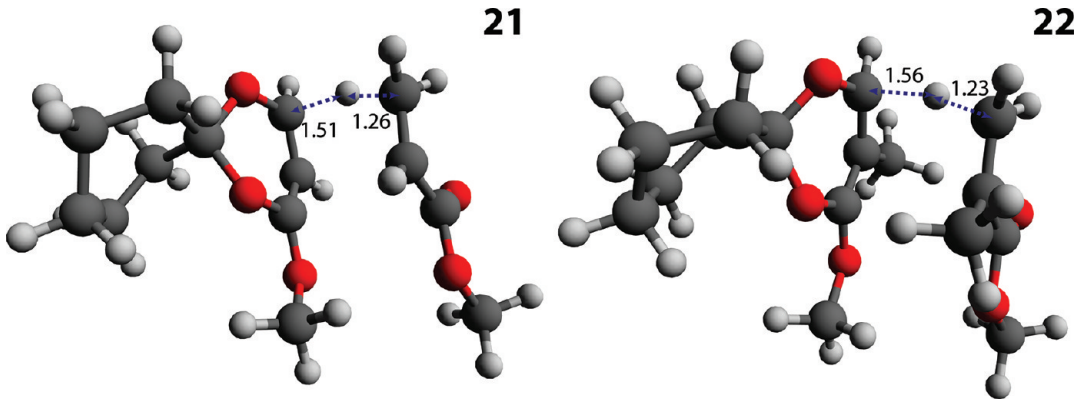


**Figure 11. 21**: transition state of hydrogen transfer reaction from MA−CHo DAA to MA. **22**: transition state of hydrogen transfer reaction from MMA−CHo DAA to MMA. All interatomic lengths are in Å.

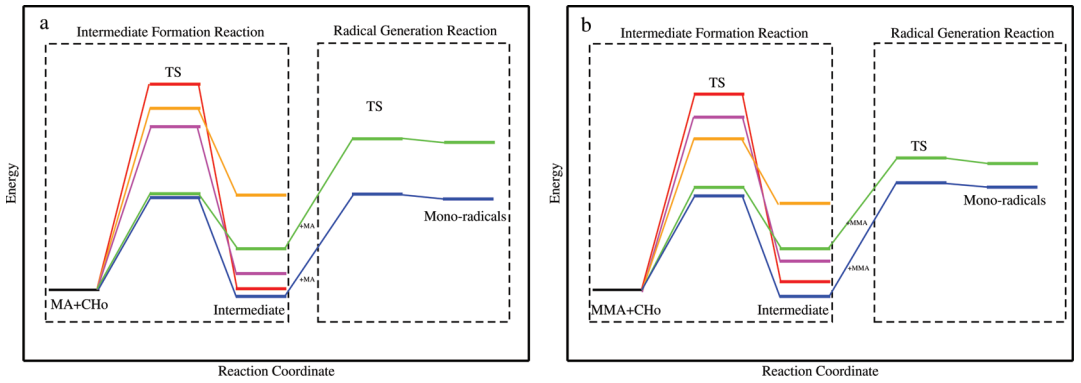


**Figure 12.** Comparison of the four mechanisms: (a) reaction of MA and CHo; (b) reaction of MMA and CHo. Key: orange, modified Kaim mechanism; magenta, 2,2,3-cycloaddition (2,2,3,3-cycloaddition); red, 2,2,4-cycloaddition (2,2,4,4-cycloaddition); blue, complexation-involved hydrogen transfer reaction; green, Mayo mechanism.

Markovnikov hydrogen transfer from CHo to MA. The contour is constructed from single point energy calculations by constraining $r$(C3−H4) and $r$(C5−H4) from 1.09 to 3.89 Å, respectively. We found that the energy barrier for the formation of monoradicals from reactants is greater than 350 kJ/mol. The reverse reaction, from monoradicals to CHo and MA (reactants), was found to be barrierless, which agrees with previous report[49] that shows radical disproportionation usually has no energy barrier. The Mulliken charge on C3 of CHo was calculated to be −0.351 and those of C5 and C6 of MA −0.301 and −0.13, respectively. The higher electron density of C3 compared to those of C5 and C6 indicates that these two carbon atoms are not sufficiently reactive (electronegative) to abstract the $\alpha$-position hydrogen from CHo, and that the direct hydrogen addition is not a likely mechanism.

The complexation reaction was studied by imposing three constraints: 1.09 Å < $r$(C3−H4) < 1.60 Å, 1.09 Å < $r$(H4−C5) < 1.60 Å, 1.55 Å < $r$(O1−C6) < 2.20 Å for Markovnikov addition and 1.09 Å < $r$(C3−H4) < 1.60 Å, 1.09 Å < $r$(H4−C6) < 1.60 Å, 1.55 Å < $r$(O1−C5) < 2.20 Å for anti-Markovnikov addition. Mulliken charge analysis shows that the interaction between O1 and C5 (C6) increases the electron density of C6 (C5) and, as a consequence, the ability of C6 (C5) to abstract the hydrogen atom. Figure 7 shows the transition states of the complexation reaction in MA and MMA. Table 3 gives the calculated energy barriers and rate constants. It can be seen from Table 3 that the hydrogen prefers to transfer to $CH_2$-end, in agreement with the Markovnikov rules, and the activation energies of both reactions are lower than that for intermediate formation in the modified Kaim's mechanism.

Monoradical formation via thermal dissociation of the intermediate was found to be improbable due to the strong chemical bond between O1 and C5 (C6) in the intermediate. Instead, we find that the intermediate can produce mono-radicals by donating a hydrogen atom to a monomer, as shown in Figure 8. We estimated the activation energy using B3LYP/6-31G* for the radical generation reactions to be 132.2 kJ/mol for the $CH_2$-end added MA−CHo intermediate and 160.8 kJ/mol for the $CH_2$-end added MMA−CHo intermediate, respectively (Table 4). These suggest that the $\alpha$-position hydrogen transfer is a possible initiation mechanism in thermal polymerization of MA and MMA in CHo.

**3.4. Mayo Mechanism.** The Mayo mechanism presented in Figure 1(IV) is a thermal cycloaddition [4+2] reaction. The reaction between the carbonyl group of a CHo and the conjugated O═C—C═C of one vinyl monomer was studied by constraining 1.45 Å < $r$(C2—O8) < 2.20 Å and 1.45 Å < $r$(O1—C5) < 2.20 Å. Concerted transition states, **17** in MA and **18** in MMA, were identified for the formation of Diels−Alder Adducts (DAAs), **19** and **20**, respectively, as shown in Figure 9. Table 5 gives the energy barriers and rate constants for the formation of the DAAs. The activation energies for the formation of MA−CHo DAA (133 kJ/mol) and MMA−CHo DAA (141 kJ/mol) were found to be comparable to that of DAA formation in monomer self-initiation of styrene (110.4 kJ/mol with B3LYP/6-31G* using UHF wave functions).[41]


dx.doi.org/10.1021/jp2124394 | J. Phys. Chem. A 2012, 116, 5337−5348

The activation energy for the monoradical generation reaction shown in Figure 10 was calculated using B3LYP/6-31G*. The energy barriers are 118.9 and 128.0 kJ/mol for MA−CHo DAA and MMA−CHo DAA, respectively (Table 4). Figure 11 depicts the transition-state structures for the monoradical generation reaction. It is important to note that the monoradical generation mechanism is comparable to the molecular assisted homolysis mechanism reported for the self-initiation in styrene.[41] The estimated relative rate coefficient ($k_r$) compared to monomer self-initiation[23,26] for the overall reaction, the intermediate formation and the subsequent radical generation reaction, is provided in Table 4.

The activation energies for the formation of DAA and $CH_2$-end added intermediate in the hydrogen transfer reaction are comparable. The energy barrier for the monoradical generation reaction from the DAA is about 25 kJ/mol less than that from the $CH_2$-end added intermediate. This suggests that both complexation-involved hydrogen transfer and Mayo mechanism are much more likely to produce monoradicals.

## 4. CONCLUSIONS

Four different mechanisms of initiation in spontaneous thermal homo-polymerization of methyl acrylate and methyl methacrylate in cyclohexanone were explored. The results are summarized in Figure 12. We found that the modified Kaim mechanism was not likely to be causing initiation, due to the higher activation energy for the intermediate formation reaction and the inability of the intermediate to decompose and release monoradicals for initiation. The Flory mechanism was also found to be incapable of generating monoradicals due to the inability of the singlet diradical species in 2,2,3-cycloaddition (2,2,3,3-cycloaddition) to undergo crossover to reactive triplet states and the significantly higher activation energies of the 2,2,4-cycloaddition (2,2,4,4-cycloaddition) route. The complexation-involved hydrogen transfer reaction was identified to be probable to initiate polymerization due to the capability of the intermediate to donate a hydrogen and form monoradicals. We determined that the Mayo mechanism can form the DAA intermediate, which can subsequently donate a hydrogen to a second monomer to produce radical species for initiating polymerization. The barriers for the formation of the DAA and the $CH_2$-end added intermediate were found to be comparable. In view of these, we suggest that the Mayo and complexation-involved hydrogen transfer mechanisms are both capable of generating monoradicals in thermal homo-polymerization of methyl acrylate and methyl methacrylate in cyclohexanone.

## ■ ASSOCIATED CONTENT

### Supporting Information

Coordinates of structures shown in the paper, energy of reactants, transition states and products in Hartrees, imaginary frequencies in $cm^{-1}$, raw data for Figure 6, and Eckart tunneling correction. The coordinates corresponding to the 2D contour plot (Figure 6) are also presented. The Eckart tunneling correction is briefly discussed. This information is available free of charge via the Internet at http://pubs.acs.org

## ■ AUTHOR INFORMATION

### Corresponding Author

*E-mail: rappe@sas.upenn.edu.

### Notes

The authors declare no competing financial interest.

## ■ ACKNOWLEDGMENTS

S.S. and M.S. acknowledge the National Science Foundation (NSF) through Grant CBET-0932882. Acknowledgment is also made to the Donors of the American Chemical Society Petroleum Research Fund for partial support of this research. S.L. acknowledges the NSF through the grant CBET-0932786, and A.M.R. acknowledges the Air Force Office of Scientific Research, through grant FA9550-10-1-0248. Computational support was provided by the High-Performance Computing Modernization Office of the U.S. Department of Defense.

## ■ REFERENCES

(1) Weiss, K. D. *Prog. Polym. Sci.* **1997**, *22*, 203−245.
(2) Sorensen, P. A.; Kiil, S.; Dam-Johansen, K.; Weinell, C. E. *J. Coat. Technol. Res.* **2009**, *6*, 135−176.
(3) Adamsons, K.; Blackman, G.; Gregorovich, B.; Lin, L.; Matheson, R. *Prog. Org. Coat.* **1998**, *34*, 64−74.
(4) Wang, W.; Hutchinson, R. A. *Chem. Eng. Technol.* **2010**, *33*, 1745−1753.
(5) Li, D. H.; Grady, M. C.; Hutchinson, R. A. *Ind. Eng. Chem. Res.* **2005**, *44*, 2506−2517.
(6) Rantow, F. S.; Soroush, M.; Grady, M. C.; Kalfas, G. A. *Polymer* **2006**, *47*, 1423−1435.
(7) Grady, M. C.; Simonsick, W. J.; Hutchinson, R. A. *Macromol. Symp.* **2002**, *182*, 149−168.
(8) Quan, C. L.; Soroush, M.; Grady, M. C.; Hansen, J. E.; Simonsick, W. J. *Macromolecules* **2005**, *38*, 7619−7628.
(9) Zorn, A. M.; Junkers, T.; Barner-Kowollik, C. *Macromol. Rapid Commun.* **2009**, *30*, 2028−2035.
(10) Walling, C.; Briggs, E. R.; Mayo, F. R. *J. Am. Chem. Soc.* **1946**, *68*, 1145−1149.
(11) Stickler, M.; Meyerhoff, G. *Makromol. Chem.* **1978**, *179*, 2729−2745.
(12) Lingnau, J.; Stickler, M.; Meyerhoff, G. *Eur. Polym. J.* **1980**, *16*, 785−791.
(13) Stickler, M.; Meyerhoff, G. *Makromol. Chem.* **1980**, *181*, 131−147.
(14) Stickler, M.; Meyerhoff, G. *Polymer* **1981**, *22*, 928−933.
(15) Lingnau, J.; Meyerhoff, G. *Polymer* **1983**, *24*, 1473−1478.
(16) Lingnau, J.; Meyerhoff, G. *Macromolecules* **1984**, *17*, 941−945.
(17) Lingnau, J.; Meyerhoff, G. *Makromol. Chem.* **1984**, *185*, 587−600.
(18) Brand, E.; Stickler, M.; Meyerhoff, G. *Makromol. Chem.* **1980**, *181*, 913−921.
(19) Srinivasan, S.; Kalfas, G.; Petkovska, V. I.; Bruni, C.; Grady, M. C.; Soroush, M. *J. Appl. Polym. Sci.* **2010**, *118*, 1898−1909.
(20) Mayo, F. R. *J. Am. Chem. Soc.* **1953**, *75*, 6133−6141.
(21) Flory, P. J. *J. Am. Chem. Soc.* **1937**, *59*, 241−253.
(22) Pryor, W. A.; Lasswell, L. D. *Adv. Free-Radical Chem.* **1975**, *5*, 27−99.
(23) Srinivasan, S.; Lee, M. W.; Grady, M. C.; Soroush, M.; Rappe, A. M. *J. Phys. Chem. A* **2009**, *113*, 10787−10794.
(24) Srinivasan, S.; Lee, M. W.; Grady, M. C.; Soroush, M.; Rappe, A. M. *J. Phys. Chem. A* **2010**, *114*, 7975−7983.
(25) Zhang, C. L.; Wang, X. Y.; Liu, L. M.; Wang, Y. L.; Peng, X. Y. *J. Mol. Model.* **2008**, *14*, 1053−1064.
(26) Srinivasan, S.; Lee, M. W.; Grady, M. C.; Soroush, M.; Rappe, A. M. *J. Phys. Chem. A* **2011**, *115*, 1125−1132.
(27) Kaim, A. *J. Polym. Sci., Part A: Polym. Chem.* **1984**, *22*, 1891−1895.
(28) Kaim, A. *J. Polym. Sci. Part C: Polym. Lett.* **1984**, *22*, 203−208.
(29) Xu, Y. Q.; Xu, Q. F.; Lu, J. M.; Xia, X. W.; Wang, L. H. *Eur. Polym. J.* **2007**, *43*, 2028−2034.
(30) Ouchi, T.; Murayama, N.; Imoto, M. *Bull. Chem. Soc. Jpn.* **1980**, *53*, 748−752.
(31) Eyring, H. *J. Chem. Phys.* **1935**, *3*, 107−115.
(32) Coote, M. L. *Encycl. Polym. Sci. Technol.* **2006**, 1−57.

(33) Pfaendtner, J.; Yu, X.; Broadbelt, L. J. *Theor. Chem. Acc.* **2007**, *118*, 881−898.
(34) Van Speybroeck, V.; Van Neck, D.; Waroquier, M.; Wauters, S.; Saeys, M.; Marin, G. B. *J. Phys. Chem. A* **2000**, *104*, 10939−10950.
(35) Van Speybroeck, V.; Van Cauter, K.; Coussens, B.; Waroquier, M. *ChemPhysChem* **2005**, *6*, 180−189.
(36) Lin, C. Y.; Izgorodina, E. I.; Coote, M. L. *J. Phys. Chem. A* **2008**, *112*, 1956−1964.
(37) Yu, X. R.; Pfaendtner, J.; Broadbelt, L. J. *J. Phys. Chem. A* **2008**, *112*, 6772−6782.
(38) Thickett, S. C.; Gilbert, R. G. *Polymer* **2004**, *45*, 6993−6999.
(39) Srinivasan, S. *Ph.D. Thesis*, Drexel University, Philadelphia, PA, 2009.
(40) Srinivasan, S.; Moghaddam, N.; Soroush, M.; Grady, M. C.; Rappe, A. M. *AIChE Annual Meeting* **2010**.
(41) Khuong, K. S.; Jones, W. H.; Pryor, W. A.; Houk, K. N. *J. Am. Chem. Soc.* **2005**, *127*, 1265−1277.
(42) Irikura, K. K. *THERMO.PL*; National Institute of Standards and Technology: Gaithersburg, MD, 2002
(43) http://cccbdb.nist.gov.
(44) Wigner, E. *J. Chem. Phys.* **1937**, *5*, 720−725.
(45) Eckart, C. *Phys. Rev.* **1930**, *35*, 1303−1309.
(46) Duncan, W. T.; Bell, R. L.; Truong, T. N. *J. Comput. Chem.* **1998**, *19*, 1039−1052.
(47) Yu, Y. X.; Li, S. M.; Xu, Z. F.; Li, Z. S.; Sun, C. C. *Chem. Phys. Lett.* **1999**, *302*, 281−287.
(48) Schmidt, M. W.; Baldridge, K. K.; Boatz, J. A.; Elbert, S. T.; Gordon, M. S.; Jensen, J. H.; Koseki, S.; Matsunaga, N.; Nguyen, K. A.; Su, S. J.; Windus, T. L.; Dupuis, M.; Montgomery, J. A. *J. Comput. Chem.* **1993**, *14*, 1347−1363.
(49) de Bruin, T. J. M.; Lorant, F.; Toulhoat, H.; Goddard, W. A. *J. Phys. Chem. A* **2004**, *108*, 10302−10310.